Nanoscale Res Lett (2009) 4:802–808
DOI 10.1007/s11671-009-9318-6

NANO EXPRESS

Synthesis of Novel Double-Layer Nanostructures of SiC–WO_x by a Two Step Thermal Evaporation Process

Hyeyoung Kim · Karuppanan Senthil · Kijung Yong

Received: 15 February 2009 / Accepted: 6 April 2009 / Published online: 19 April 2009

Abstract A novel double-layer nanostructure of silicon carbide and tungsten oxide is synthesized by a two-step thermal evaporation process using NiO as the catalyst. First, SiC nanowires are grown on Si substrate and then high density $W_{18}O_{49}$ nanorods are grown on these SiC nanowires to form a double-layer nanostructure. XRD and TEM analysis revealed that the synthesized nanostructures are well crystalline. The growth of $W_{18}O_{49}$ nanorods on SiC nanowires is explained on the basis of vapor–solid (VS) mechanism. The reasonably better turn-on field (5.4 V/μm) measured from the field emission measurements suggest that the synthesized nanostructures could be used as potential field emitters.

Keywords Silicon carbide · Tungsten oxide · Nanowires · Nanorods · Vapor–solid mechanism · Field emission

Introduction

The one-dimensional (1D) semiconductor nanostructures have attracted considerable research activities not only because of their interesting electronic and optical properties intrinsically associated with their low dimensionality and the quantum confinement effect but also because of their potential applications in electronic and optoelectronic nanoscale devices [1–4]. Recently, heteronanostructures of various functional materials have attracted increasing attention in materials chemistry and nanoscience because of their many desirable properties, which can be tailored by fine-tuning the composition, morphology, size and self-assembly of nanosized building blocks for the fabrication of functional electronic and photonic devices [5–9]. These heteronanostructured materials provide the opportunity to study the properties of material combinations that are difficult or impossible to fabricate in the bulk. Considerable effort has been made in recent years to synthesize various types of heteronanostructures such as superlattice structures [9, 10], core-shell structures [11–14], coaxial or biaxial nanostructures [15–17], hierarchical heterostructures [18–22], and 1D heteronanostructures [23–25]. Various growth techniques have been employed including laser-assisted catalytic growth, chemical vapor deposition (CVD), metal–organic chemical vapor deposition (MOCVD), and thermal evaporation to fabricate various 1D semiconductor heteronanostructures [9–25]. Although significant advances have been made in the fabrication of simple binary semiconducting nanostructures, direct fabrication of complex heteronanostructures with controlled morphology, size, and composition remains still challenging.

Tungsten oxide is an *n*-type wide band gap (3.25 eV) semiconductor with a work function in the range of 5.59–5.70 eV which makes it attractive for the field emission applications. One-dimensional nanomaterials of tungsten oxide (WO_3) and its sub-oxides (WO_x) have been intensively studied due to their excellent physical and chemical properties for various potential applications as field

Hyeyoung Kim and Karuppanan Senthil contributed equally to this article.

H. Kim · K. Yong (✉)
Department of Chemical Engineering, Pohang University of Science and Technology (POSTECH), San 31, Hyoja-dong, Nam-gu, Pohang 790-784, South Korea
e-mail: kyong@postech.ac.kr

K. Senthil
Center for Information Materials, Pohang University of Science and Technology (POSTECH), San 31, Hyoja-dong, Nam-gu, Pohang 790-784, South Korea

emitters, electro-chromic devices, semiconductor gas sensors, catalysts, information displays, and smart windows [26–30]. Silicon carbide is a wide band gap (2.3 eV) semiconductor with many interesting properties, such as high hardness, large thermal conductivity, a low coefficient of thermal expansion, and excellent resistance to erosion and corrosion. Various SiC nanostructures have attracted much attention in recent years due to their potential application in nanocomposite materials and microelectronic devices [31–33]. Because of their promising physical and electrical properties, nanostructures of tungsten oxide and silicon carbide might play a crucial role as the building blocks in the fabrication of functional heteronanostructures. Although the growth of different types of WO_3 and SiC nanostructures have been reported in recent years, there are only few reports available on the heteronanostructures of WO_3 and SiC with other materials. Chen and Ye [18] have reported the synthesis and photocatalytic properties of novel 3D hierarchical WO_3 hollow shells, including hollow dendrites, spheres, and dumbbells, self organized from tiny WO_3 nanoplatelets. Hierarchical heteronanostructure of W nanothorns on WO_3 nanowhiskers (WWOs) was fabricated by Baek et al. [20] by a simple two-step evaporation process and the hierarchical WWOs were found to exhibit promising field emission properties. Tak et al. [34] synthesized heteronanojunction of ZnO nanorods on SiC nanowires by a combination of thermal evaporation and MOCVD process. Bae et al. [25] have fabricated heterostructures of ZnO nanorods with various 1D nanostructures (CNTs, GaN, GaP, and SiC nanowires) by thermal chemical vapor deposition of Zn at a low temperature. Shen et al. [35] have synthesized hierarchical SiC nanoarchitectures by a simple chemical vapor deposition process and reported their field emission properties. Since there are no reports available on the heteronanostructures of WO_3 with SiC up to our knowledge, in this article, we report for the first time, the synthesis of SiC–WO_x nanostructures by a simple two-step thermal evaporation process. We synthesized a novel double-layer SiC–WO_x nanostructure with $W_{18}O_{49}$ nanorods on SiC nanowires.

Experimental

Synthesis of SiC–WO_x Double-Layer Nanostructures

The growth of 1D SiC–$W_{18}O_{49}$ double-layer nanostructure was achieved by a simple two step evaporation process. The first step was the growth of SiC nanowires on Si(100) substrates to serve as the substrate for the growth of WO_x nanostructures. The second step was to grow $W_{18}O_{49}$ nanorods on the SiC nanowires to obtain SiC–WO_x double-layer nanostructures.

Synthesis of SiC Nanowires (1st step)

First, core-shell SiC–SiO_2 nanowires were grown on Si(100) substrates by carbothermal reaction of tungsten oxide (WO_3) with graphite (C) using NiO catalyst [36]. The substrates used in our experiment were highly doped (0.003 Ω-cm) *n*-type Si(100) wafers. The Si substrates were dipped in the $Ni(NO_3)_2$/ethanol solution (0.06 M) after being cleaned in an ultrasonic acetone bath for 20 min and then dried in the oven at 60 °C for 15 min. WO_3 and C mixed powders were placed in an alumina boat and $Ni(NO_3)_2$-coated Si substrate was kept on the top of the boat. Then the source–substrate containing alumina boat was kept at the uniform temperature zone of the furnace. After the residual air in the furnace quartz tube was eliminated with Ar gas flow for 30 min, the furnace temperature was increased to about 1100 °C under a constant Ar flow of 500 sccm. Then the furnace temperature was maintained at 1100 °C for 3 h to grow core-shell SiO_2–SiC nanowires. After cooling down to room temperature, the surface of the Si substrate was covered with a white colored deposit. The substrates with core-shell SiO_2–SiC nanowires were etched in HF aqueous solution (49% HF:H_2O = 1:4) for 3 min to remove the SiO_2 shell layer.

Synthesis of SiC–WO_x Nanostructures (2nd step)

The synthesized HF-etched SiC nanowire samples were dipped in the $Ni(NO_3)_2$/ethanol solution (0.06 M) twice and then dried in the oven. High purity (Aldrich, 99.99%) WO_3 powder, deposited on the edge of an alumina boat, acted as the source material for the tungsten oxide nanorod growth. Then the SiC nanowire sample was placed on the top of the alumina boat with the SiC deposited side facing the source material. After evacuating the furnace to a vacuum of 100 mTorr, the temperature of the furnace was slowly increased from room temperature to the growth temperature of 1050 °C and the temperature was maintained constant for 1 h. After the growth process, the furnace was allowed to cool normally to room temperature. The surface of the substrate with white colored deposit became blue after tungsten oxide deposition and the obtained SiC–WO_x double-layer nanostructures were characterized by using various techniques.

Characterization of SiC–WO_x Double-Layer Nanostructures

The synthesized SiC–WO_x double-layer nanostructures were characterized by using field-emission scanning electron microscopy (FE-SEM; JEOL JSM 330F), X-ray diffraction (XRD; Rigaku D-Max1400, Cu$K\alpha$ radiation λ = 1.5406 Å), high-resolution transmission electron

microscopy (HR-TEM; JEOL 2100F, accelerating voltage 200 kV, resolution 0.14 nm lattice), high-resolution scanning transmission electron microscope (HR-STEM), energy-dispersive X-ray spectroscopy (EDX), and field emission measurements.

Results and Discussion

Figure 1a shows the surface morphology of the SiC–WO_x nanostructures examined by scanning electron microscopy (SEM). The SEM image clearly shows that the synthesized SiC–WO_x nanostructures are of double layer structures. The top of the SiC nanowires are covered uniformly by the high density WO_x nanorods. The magnified images shown in Fig. 1b and c correspond to the SEM images from WO_x and SiC nanostructures, respectively. The morphology of the WO_x nanostructures is found to have rod-like structures with 100–400 nm in diameter and several micrometers in length. The SEM image of SiC nanowires shows that there are large amount of straight, curved, and randomly oriented and freestanding nanowires. SiC nanowires are of several tens of micrometers in length and 20–50 nm in diameter. The HRTEM lattice images from the WO_x and SiC nanowires are shown in Fig. 1d and e, respectively. The clear stripes of lattice planes indicate that the grown nanostructures are highly crystalline. The spacing of the lattice fringes measured from the HRTEM lattice image of WO_x is found to be 0.379 nm and this is in excellent agreement with the standard *d*-value of (010) plane of a monoclinic $W_{18}O_{49}$ crystal, according to the JCPDS card No. 71-2450. The HRTEM lattice image of SiC shows a lattice fringe spacing of 0.248 nm, which can be indexed to the (111) plane of cubic SiC, according to the JCPDS card No. 29-1129.

Figure 2 shows the XRD pattern obtained from the SiC–WO_x double-layer nanostructures, indicating that both the WO_x (marked green) and SiC (marked red) nanostructures

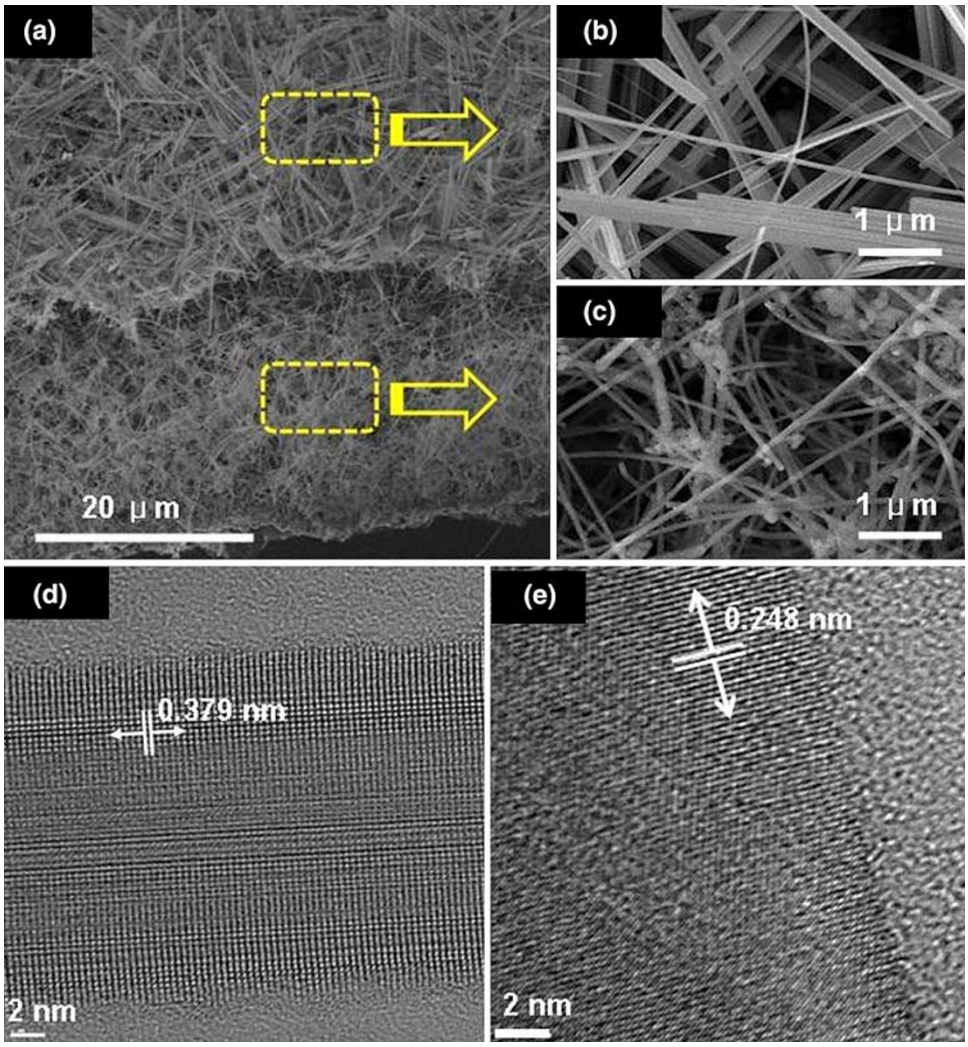

Fig. 1 **a** SEM image obtained from SiC–$W_{18}O_{49}$ nanostructures (cross-sectional view); **b**, **c** magnified image of (**a**) corresponding to $W_{18}O_{49}$ nanorod layer and SiC nanowire layer, respectively; **d** HR-TEM lattice image from $W_{18}O_{49}$ nanorod; and **e** HR-TEM lattice image from SiC nanowire

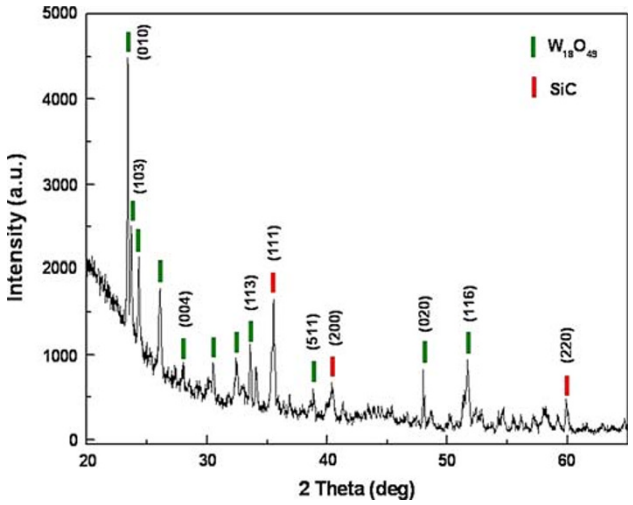

Fig. 2 X-ray diffraction pattern from SiC–$W_{18}O_{49}$ double-layer nanostructures

are highly crystallized. All the diffraction peaks can be indexed to monoclinic $W_{18}O_{49}$ (JCPDS card No: 71-2450) and cubic SiC nanowires (29-1129).

Figures 3a and b shows the low magnification TEM images of the SiC–WO_x nanostructures. TEM images did not show any junction between the $W_{18}O_{49}$ and SiC nanostructures. The TEM images show that $W_{18}O_{49}$ nanorod is smooth and straight without any particles. SiC nanowires are curved and there are few particles at some portion of the nanowires. The EDX analysis on these SiC nanowires showed that the particles are composed of W and O. The microscopic structure and chemical composition of SiC nanowires with few particles are investigated using a high-resolution scanning transmission electron microscope (HR-STEM). Figure 3c shows the high angle annular dark field (HAADF) STEM image from the SiC–WO_x nanostructures. It was observed that there are some particles on the surface of the SiC nanowires. Figure 3d–f show corresponding EELS elemental mapping of Si, W, and O, respectively. The signal from C is not shown here since C signals come from the TEM grid also. The presence of W and O on the SiC nanowire surface suggests that the $W_{18}O_{49}$ nanorods start to grow on the SiC nanowire surface with NiO as the catalyst. In a typical vapor–liquid–solid (VLS) mechanism, the catalyst particles are usually found at the top or bottom of the nanostructures. However, $W_{18}O_{49}$ nanorods synthesized in this study do not have any catalyst particles (NiO or Ni) on its surface. Instead, the vapor–solid (VS) mechanism might be responsible for the growth of $W_{18}O_{49}$ nanorods on SiC nanowire surfaces. When the temperature of the furnace is increased to high temperature, the tungsten oxide vapor will be continuously generated from the source. The generated vapor source becomes supersaturated for nucleation of small clusters and tungsten oxide is nucleated on the top of the SiC nanowire surface by VS mechanism. Thus, high density $W_{18}O_{49}$ nanorods are grown uniformly on the SiC nanowires, which acted as the substrate. The observation of SiC and $W_{18}O_{49}$ nanostructures separately in the TEM image indicates that the bonding between these two nanostructures might be weak and so they might have been detached during the sample preparation for TEM measurements. We could not observe uniform and high density tungsten oxide nanorods when NiO catalyst was not used before the growth of tungsten oxide. This might be due to the fact that NiO coated surface enhances the nucleation of tungsten oxide when compared with the uncoated surface. We have successfully fabricated a new type of double-layer nanostructures by a two-step thermal evaporation process. We believe that the similar kind of growth method can be applied for other materials to grow double-layer nanostructures.

During the synthesis of WO_x nanostructures, some of the SiC nanowire samples we used are little longer than the width of the alumina boat. For these samples, end parts of the SiC nanowire surface do not face the tungsten oxide source material. The center part of the sample is very close to the source material and the end part is away from the source material. Interestingly, we observed a mass transport effect during the growth of WO_x nanostructures under this condition. Figure 4a shows the digital photograph image of the SiC–$W_{18}O_{49}$ double-layer nanostructure sample showing the mass transport effect. The image clearly shows the three different regions having different densities of $W_{18}O_{49}$ nanorods. Figure 4b–d shows the SEM images from the three regions of the sample showing variation in the density of $W_{18}O_{49}$ nanorods. The sample part (Fig. 4d) showing the high density $W_{18}O_{49}$ nanorods is placed very close to the source whereas the sample part (Fig. 4b) showing only SiC nanowires is away from the source material and so there is no tungsten oxide growth. Thus the density of nanorods decreased gradually from the center to the end of the sample, owing to the mass transport of tungsten oxide source material. These kinds of nanostructures showing density gradient within the sample might be useful for some specific applications because of their different optical and electrical properties.

The field emission measurements were performed inside a vacuum chamber of pressure below 1×10^{-6} Torr. The Si substrate with SiC–$W_{18}O_{49}$ double-layer nanostructures was used as the cathode and indium tin oxide (ITO) coated glass plate was used as the anode. The cathode to anode distance was maintained at 100 μm for all the measurements. The emission current was measured as a function of applying voltage (voltage range of 100–750 V in steps of 10 V) after sweeping the voltage several times. During sweeping voltages, the adsorbates from the emitter surface are desorbed and the field emission becomes stable after several cycles. Figure 5, shows the emission current

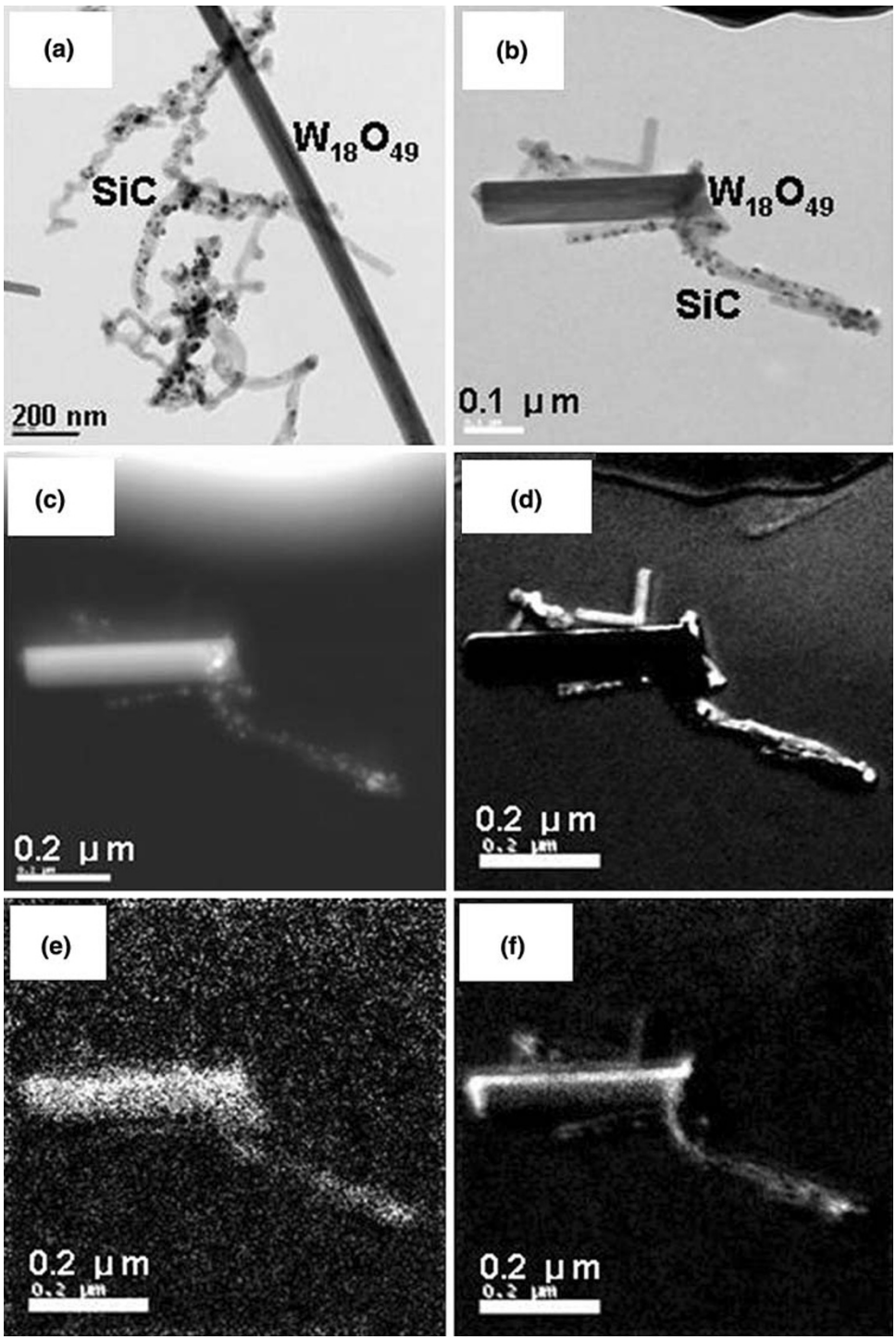

Fig. 3 **a**, **b** Low-magnification TEM images of SiC–$W_{18}O_{49}$ double-layer nanostructures showing $W_{18}O_{49}$ and SiC separately; **c** high angle annular dark field (HAADF) STEM image of SiC nanowires with some particles; and corresponding EELS elemental mapping of **d** Si, **e** W, and **f** O, respectively

density (J) versus applied field (E). Here, we define the turn-on field as the electric field required to produce a current density of 10 μA/cm^2. It is found that apparent turn-on field was 5.4 V/μm. The field emission performance is compared with our previously reported results for WO_x and SiC nanostructures. The obtained turn-on field is lower than that of our earlier reported values for $W_{18}O_{49}$ nanowires (9.5 V/μm) [37], W/WO_3 heteronanostructures (6.2 V/μm) [20], and slightly higher than that of WO_3 nanowires (4.8 V/μm) [38], SiC nanowires (2–5 V/μm) [36, 39]. The turn-on field value is comparable with many other types of nanostructures such as BN nanosheets aligned Si_3N_4 nanowires (4.2 V/μm) [40], hierarchical AlN nanostructures (2.5–3.8 V/μm) [21], BN coated SiC nanowires (6 V/μm) [41], ZnS-In core-shell heteronanostructures (5.4–5.6 V/μm) [42], and hierarchical SiC

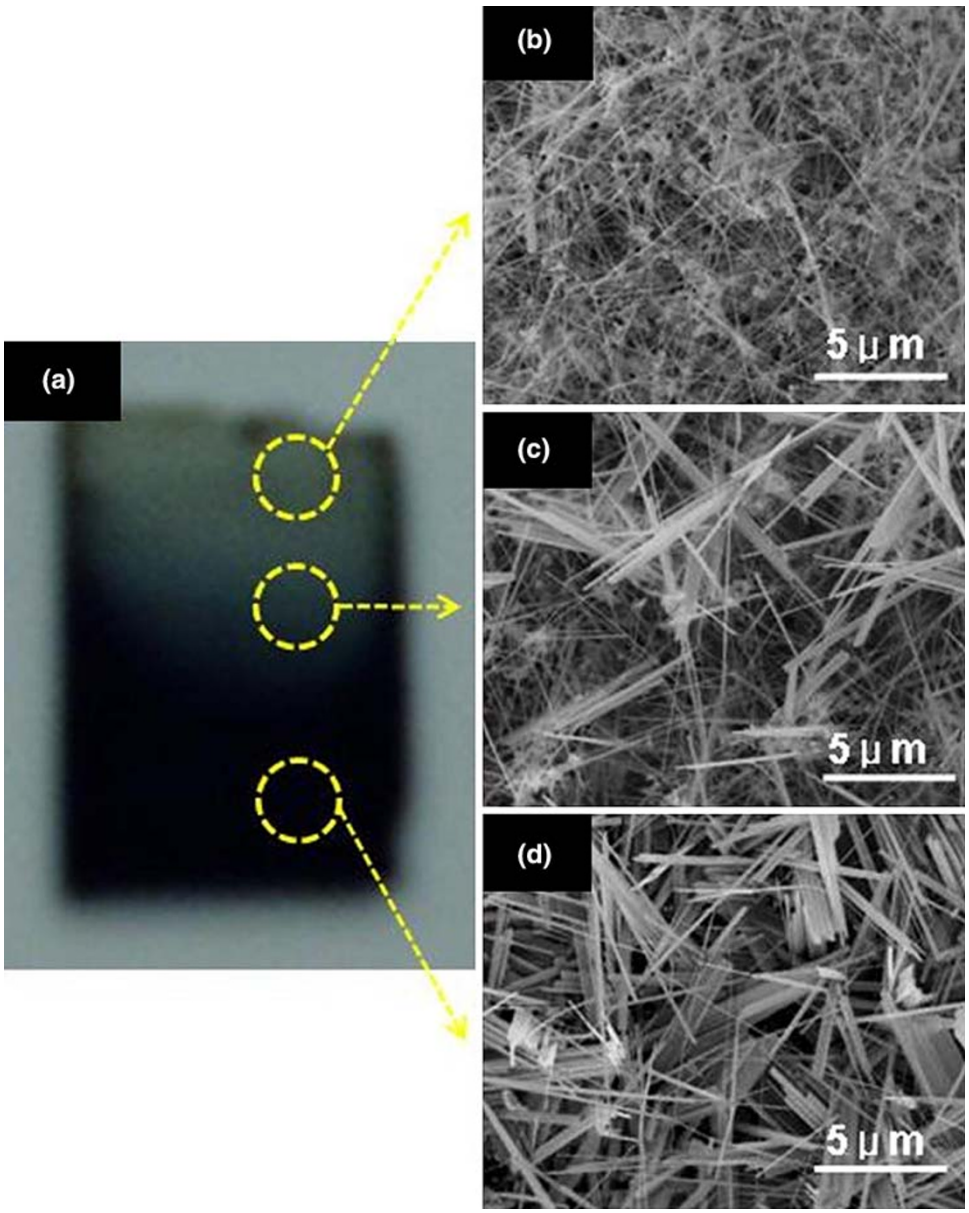

Fig. 4 **a** Digital camera image of a SiC–$W_{18}O_{49}$ double-layer nanostructure sample showing density gradient owing to mass transport of tungsten oxide source material; and **b–d** SEM image from different regions of the sample having only SiC nanowires, low density $W_{18}O_{49}$ and high density $W_{18}O_{49}$ nanorods, respectively

nanostructures (12 V/μm) [35]. The reasonably better turn-on field for our nanostructures indicates that both the SiC and $W_{18}O_{49}$ nanostructures contribute to the field emission process and also it shows that both the nanostructures have good electrical bonding. The inset of Fig. 5 shows a typical Fowler–Nordheim (F–N) plot for our SiC–$W_{18}O_{49}$ nanostructures. The linearity of this curve shows that a conventional F–N mechanism was responsible for the field emission from our samples.

Conclusions

We report, for the first time, the synthesis of new type of nanostructures comprising silicon carbide and tungsten oxide by a simple two step thermal evaporation process. The synthesized nanostructures are double-layer SiC–$W_{18}O_{49}$ nanostructure. Based on TEM and EDX analysis, a possible VS growth mechanism was proposed for the grown double-layer nanostructure. At some certain conditions, we observed that $W_{18}O_{49}$ nanorods having different density (density gradient) can be grown on the SiC nanowires and this is attributed to the mass transport effect of tungsten oxide source material. This simple method of fabricating a new type of double-layer nanostructures with one of the nanostructures acting as substrate for the growth of other nanostructure could be applied to other materials to create heteronanostructures for device applications. Field emission measurements showed that the fabricated double-layer nanostructures are good field emitters.

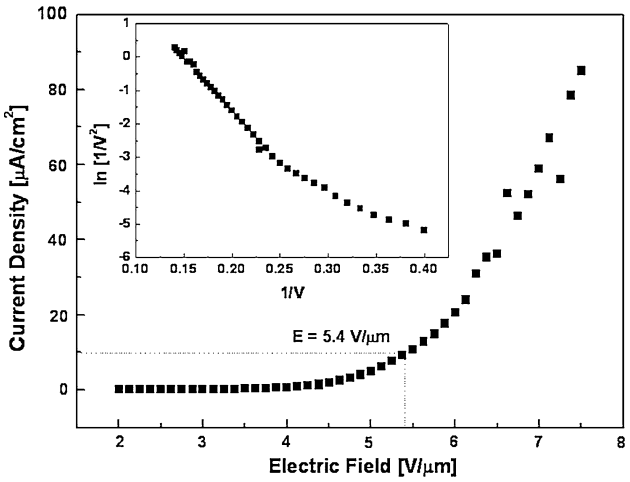

Fig. 5 Field emission characteristics (current density–electric field) of SiC–$W_{18}O_{49}$ double-layer nanostructures. The inset is the corresponding Fowler–Nordheim (F–N) plot

Acknowledgments This work was supported by grant No. RT104-01-04 from the Regional Technology Innovation Program of the Ministry of Commerce, Industry and Energy (MOCIE), and the Korean Research Foundation Grants funded by the Korean Government (MOEHRD) (KRF-2008-005-J00501).

References

1. C.M. Lieber, Z.L. Wang, MRS Bull. **32**, 99 (1997)
2. Y. Jiang, W.J. Zhang, J.S. Jie, X.M. Meng, J.A. Zaipen, S.T. Lee, Adv. Mater. **18**, 1527 (2006). doi:10.1002/adma.200501913
3. Y. Xia, P. Yang, Y. Sun, Y. Wu, B. Mayers, B. Gates, Y. Yin, F. Kim, H. Yan, Adv. Mater. **15**, 353 (2003). doi:10.1002/adma.200390087
4. X.F. Duan, Y. Huang, Y. Cui, J.F. Wang, C.M. Lieber, Nature **409**, 66 (2001). doi:10.1038/35051047
5. J. Zhou, J. Liu, X. Wang, J. Song, R. Tummala, N.S. Xu, Z.L. Wang, Small **3**, 622 (2007). doi:10.1002/smll.200600495
6. Y. Wu, J. Xiang, C. Yang, W. Lu, C.M. Lieber, Nature **430**, 61 (2004). doi:10.1038/nature02674
7. C. Thelander, T. Martensson, M.T. Bjork, B.J. Ohlsson, M.W. Larsson, L.R. Wallenberg, L. Samuelson, Appl. Phys. Lett. **83**, 2052 (2003). doi:10.1063/1.1606889
8. M.T. Bjork, B.J. Ohlsson, C. Thelander, A.I. Persson, K. Deppert, L.R. Wallenberg, L. Samuelson, Appl. Phys. Lett. **81**, 4458 (2002). doi:10.1063/1.1527995
9. M.S. Gudiksen, L.J. Lauhon, J.F. Wang, D.S. Smith, C.M. Lieber, Nature **415**, 617 (2002). doi:10.1038/415617a
10. Y. Wu, R. Fan, P. Yang, Nano Lett. **2**, 83 (2002). doi:10.1021/nl0156888
11. M. Chen, L. Gao, S. Yang, J. Sun, Chem. Commun. 1272 (2007)
12. O. Hayden, A.B. Greytak, D.C. Bell, Adv. Mater. **17**, 701 (2005). doi:10.1002/adma.200401235
13. J. Cao, J.Z. Sun, J. Hong, H.Y. Li, H.Z. Chen, M. Wang, Adv. Mater. **16**, 84 (2002). doi:10.1002/adma.200306100
14. L.J. Lauhon, M.S. Gudiksen, D. Wang, C.M. Lieber, Nature **420**, 57 (2002). doi:10.1038/nature01141
15. L.W. Yin, M.S. Li, Y. Bando, D. Golberg, X. Yuan, T. Sekiguchi, Adv. Funct. Mater. **17**, 270 (2007). doi:10.1002/adfm.200600065
16. D.W. Kim, I.S. Hwang, S.J. Kwon, H.Y. Kang, K.S. Park, Y.J. Choi, K.J. Choi, J.G. Park, Nano Lett. **7**, 3041 (2007). doi:10.1021/nl0715037
17. C. Wang, J. Wang, Q. Li, G.C. Yi, Adv. Funct. Mater. **15**, 1471 (2005). doi:10.1002/adfm.200400564
18. D. Chen, J. Ye, Adv. Funct. Mater. **18**, 1 (2008)
19. L. Xu, Y. Su, S. Li, Y. Chen, Q. Zhou, S. Yin, Y. Feng, J. Phys. Chem. B **111**, 760 (2007). doi:10.1021/jp066609p
20. Y. Baek, Y. Song, K. Yong, Adv. Mater. **18**, 3105 (2006). doi:10.1002/adma.200601021
21. L.W. Yin, Y. Bando, Y.C. Zhu, M.S. Li, Y.B. Li, D. Golberg, Adv. Mater. **17**, 110 (2005). doi:10.1002/adma.200400504
22. J.Y. Lao, J.G. Wen, Z.F. Ren, Nano Lett. **2**, 1287 (2002). doi:10.1021/nl025753t
23. S. Sun, G. Meng, G. Zhang, L. Zhang, Cryst. Growth Des. **7**, 1988 (2007). doi:10.1021/cg0701776
24. X.H. Sun, T.K. Sham, R.A. Rosenberg, G.K. Shenoy, J. Phys. Chem. C **111**, 8475 (2007). doi:10.1021/jp071699z
25. S.Y. Bae, H.W. Seo, H.C. Choi, J.G. Park, J.C. Park, J. Phys. Chem. B **108**, 12318 (2004). doi:10.1021/jp048918q
26. J. Chen, Y.Y. Dai, J. Luo, Z.L. Li, S.Z. Deng, J.C. She, N.S. Xu, Appl. Phys. Lett. **90**, 253105 (2007). doi:10.1063/1.2747192
27. R. Seelaboyina, J. Huang, J. Park, D.H. Kang, W.B. Choi, Nanotechnology **16**, 4840 (2006). doi:10.1088/0957-4484/17/19/010
28. C. Santato, M. Odziemkoski, M. Ulmann, J. Augustynski, J. Am. Chem. Soc. **123**, 10639 (2001). doi:10.1021/ja011315x
29. K. Sayama, K. Mukasa, R. Abe, Y. Abe, H. Arakawa, Chem. Commun. (Camb.) **23**, 2416 (2001). doi:10.1039/b107673f
30. A. Ponzoni, E. Comini, G. Sberveglieri, J. Zhou, S.Z. Deng, N.S. Xu, Y. Ding, Z.L. Wang, Appl. Phys. Lett. **88**, 203101 (2006). doi:10.1063/1.2203932
31. S.Z. Deng, Z.B. Li, W.L. Wang, N.S. Xu, J. Zhou, X.G. Zheng, H.T. Xu, J. Chen, J.C. She, Appl. Phys. Lett. **89**, 023118 (2006). doi:10.1063/1.2220481
32. W. Zhou, L. Yan, Y. Wang, Y. Zhang, Appl. Phys. Lett. **89**, 013105 (2006). doi:10.1063/1.2219139
33. W. Zhou, X. Liu, Y. Zhang, Appl. Phys. Lett. **89**, 223124 (2006). doi:10.1063/1.2398902
34. Y. Tak, Y. Ryu, K. Yong, Nanotechnology **16**, 1712 (2005). doi:10.1088/0957-4484/16/9/051
35. G. Shen, Y. Bando, D. Golberg, Cryst. Growth Des. **7**, 35 (2007)
36. K. Senthil, K. Yong, Mater. Chem. Phys. **112**, 88 (2008). doi:10.1016/j.matchemphys.2008.05.024
37. S. Jeon, K. Yong, Nanotechnology **18**, 245602 (2007). doi:10.1088/0957-4484/18/24/245602
38. Y. Baek, K. Yong, J. Phys. Chem. C **111**, 1213 (2007). doi:10.1021/jp0659857
39. Y. Ryu, Y. Tak, K. Yong, Nanotechnology **16**, S370 (2005). doi:10.1088/0957-4484/16/7/009
40. Y.C. Zhu, Y. Bando, L.W. Yin, D. Golberg, Nano Lett. **6**, 2982 (2006). doi:10.1021/nl061594s
41. C.C. Tang, Y. Bando, Appl. Phys. Lett. **83**, 659 (2003). doi:10.1063/1.1595721
42. U.K. Gautam, X.S. Fang, Y. Bando, J.H. Zhan, D. Golberg, ACS Nano. **2**, 1015 (2008). doi:10.1021/nn800013b